Inorg. Chem. **1990**, *29*, 2123–2131

Contribution from Fachbereich Chemie der Universität Marburg, Marburg, FRG, Chemistry Department, University of Tasmania,
Hobart, Tasmania 7001, Australia, Mineralogisch-Petrologisches Institut der Universität Bonn,
Bonn, FRG, and Fachbereich Physik, Universität-Gesamthochschule, Paderborn, FRG

EPR and ENDOR Spectra of Copper(II) Centers with d_{z^2} and $d_{x^2-y^2}$ Ground States in Ba_2ZnF_6: Analysis of Hyperfine Parameters and Dynamic Vibronic Coupling

Gabriele Steffen,[†] Dirk Reinen,*[,†] Horst Stratemeier,[‡] Mark J. Riley,[‡,§] Michael A. Hitchman,*[,‡]
Horst E. Matthies,[∥] Kurt Recker,*[,∥] Franz Wallrafen,[∥] and Jürgen R. Niklas*[,⊥]

Received October 2, 1989

Ba_2ZnF_6 is one of the few host lattices in which Cu^{2+} can be stabilized with a d_{z^2} ground state by isomorphous substitution of Zn^{2+} (center I). Cu^{2+} is forced to adopt a strongly tetragonally compressed octahedral coordination in this case due to the strain of the ZnF_6 host polyhedra, which are slightly distorted in the same way. EPR and ENDOR investigations, which were performed on Cu^{2+}-doped single crystals grown by the Bridgman technique, revealed the presence of a second center (II) with a $d_{x^2-y^2}$ ground state ($g_\parallel = 2.43_2$, $g_\perp = 2.07_6$). Center II was identified as Cu^{2+} on an interstitial site with a quare-planar F^- coordination, which is otherwise only known for Cu^{2+} in $CaCuF_4$. The temperature-dependent g as well as copper and fluoride hyperfine parameters of center I (4.2 K: $g_\parallel = 1.99_2$, $g_\perp = 2.36_7$) are interpreted in terms of a slight admixture of $d_{x^2-y^2}$ caused by vibronic coupling, which increases with temperature. The ground-state potential surface, the vibronic wave functions, and the corresponding energy levels have been numerically calculated. The transferred spin densities of the two centers, derived from the ligand hyperfine structure at 4.2 K (25 ± 2%) are comparable to those of Cu^{2+}-doped K_2ZnF_4 (d_{z^2} ground state). The mixing coefficients for the $d_{x^2-y^2}$ and d_{z^2} orbitals in the ground state MO's of the three centers are practically identical ($\alpha = 0.92$).

I. Introduction

Ba_2ZnF_6 is one of the few host compounds in which Cu^{2+} can be stabilized—by isomorphous substitution of Zn^{2+}—with a d_{z^2} ground state.[1] The ZnF_6 octahedra are slightly tetragonally compressed in the c direction of the unit cell (Figure 1).[2] The bonding anisotropy probably originates from the structural peculiarity in the compound, where the equatorial F^- ligands linearly bridge two Zn^{2+} ions, while the axial ligands are only involved in the coordination to the large Ba^{2+} cations. It has already been shown by EPR spectroscopy on powdered mixed crystals of $Ba_2Zn_{1-x}Cu_xF_6$ that at low Cu^{2+} concentrations the g values correspond to those that are expected for a d_{z^2} ground state and hence a tetragonally compressed Cuf_6 octahedron. The host site strain apparently determines the "sign of the Jahn–Teller distortion" at low x values (compression), while above $x \approx 0.6$, cooperative elastic interactions between neighboring CuF_6 polyhedra induced an antiferrodistortive order of elongated CuF_6 octahedra (with an orthorhombic component), in which the long Cu–F spacings are located alternately in the [100] and [010] directions of the unit cell.[3,4]

It is the intention of this paper to study the interplay between the Jahn-Teller effect and the host site strain, tending toward elongated and compressed octahedra, respectively, in a more quantitative manner on the basis of the EPR and the ENDOR spectroscopy of Cu^{2+}-doped Ba_2ZnF_6 single crystals. The temperature dependence of the g values has been interpreted in terms of the ground-state potential surface using a vibronic coupling model. A similar calculation has previously been performed for Cu^{2+} in K_2ZnF_4,[5] which has a similar layer structure, but with a much less pronounced tetragonal compression of the ZnF_6 host polyhedra.

Because Ba_2ZnF_6 is an incongruently melting compound, it was not easy to grow homogeneous single crystals. Surprisingly the crystals contained a small proportion of a second Cu^{2+} center (center II), which is not present in powder samples prepared at temperatures far below the melting point.[2] ENDOR in combination with EPR spectroscopy has been used to analyze the nature of center II, which has a $d_{x^2-y^2}$ ground state. ENDOR spectroscopy was also used to measure the fluoride hyperfine structure of this center with high resolution, which allowed the determination of the Cu → F unpaired spin density transfer with rather high precision.

II. Experimental Section

A. Single-Crystal Growth. According to the phase diagram of the system BaF_2–ZnF_2 (Figure 2)[6] the single crystal growth of the incongruently melting compound Ba_2ZnF_6 is only possible along the liquidus curve connecting the peritectic point P with the eutectic point E. The c and T values of these invariant points have been corrected by differential thermal and X-ray diffraction analysis to $T_P = 814$ °C at $c_P = 59.5$ mol % BaF_2 and $T_E = 788$ °C at $c_E = 53.5$ mol % BaF_2. Hence, for the single crystal growth of Ba_2ZnF_6, only a maximum concentration range of 6 mol % and a temperature interval of 26 °C is available, leading to a primary Ba_2ZnF_6 crystallization of 34 wt % of the ingot at most. Because of nonlinearity of the liquidus line between P and E, the undercooling and the crystallization intervals depend critically on the crucible lowering rate and the purity of the starting materials. For commercial BaF_2 and ZnF_2, special purification procedures were necessary. BaF_2 (Merck, Suprapur) was purified by Bridgman growth under vacuum [10^{-6} mbar] in graphite crucibles with addition of 1–2 wt % PbF_2 as scavenger. ZnF_2 (JMC, puratronic) was purified three to five times by fractional high-vacuum sublimation with addition of 1–5 mol % NH_4HF_2 for fluorination. Grown single crystals of the two components BaF_2 and ZnF_2 were completely transparent from the UV to the IR edge. The melting points of the purified materials were 1321 °C for BaF_2 and 947 °C for ZnF_2.

Single crystals of Ba_2ZnF_6 were grown by the Bridgman technique from nonstoichiometric melts with a starting composition of 41.5 mol% ZnF_2 and 58.5 mol % BaF_2 along the liquidus line between the peritectic point P and the eutectic point E. To find the optimum growth conditions for obtaining a maximum yield of perfect Ba_2ZnF_6 crystals, the essential parameters (temperature gradients in melt and crystal, lowering rates of the crucible, crucible materials and shapes, nucleation and seeding, and heating and cooling rates) were systematically varied. The crystal growing furnace consisted of a double-walled stainless-steel chamber, which was water-cooled and evacuable. As a resistance heater, a self-supporting bifilar graphite helix (inner diameter 40 mm, length 115 mm, wall thickness 5 mm) was used. At a growth temperature of ca. 805 °C, the temperature gradient in the zone with the highest temperature of the helix was about 65 °C/cm. The crucibles were made from spectroscopic grade graphite and had a conical tip with a capillary (diameter ≤1 mm, length 35 mm) for nucleation. The crucible lowering rates were about 0.16–0.62 mm/h. Ba_2ZnF_6 crystals were grown under vacuum (10^{-6}

---

* To whom correspondence and inquiries should be addressed: EPR spectra, D.R. or M.A.H.; preparation of the crystals, K.R.; ENDOR spectra, J.R.N.; general inquiries, D.R.

[†] Universität Marburg.

[‡] University of Tasmania.

[§] Present address: Research School of Chemistry, Australian National University, Canberra, ACT 2601, Australia.

[∥] Universität Bonn.

[⊥] Universität-Gesamthochschule Paderborn.

(1) Friebel, C.; Propach, V.; Reinen, D. *Z. Naturforsch.* **1976**, *31B*, 1574.

(2) von Schnering, H. G. *Z. Anorg. Allg. Chem.* **1967**, *353*, 13.

(3) Reinen, D.; Weitzel, H. *Z. Naturforsch.* **1977**, *32B*, 476.

(4) Reinen, D.; Friebel, C. *Struct. Bonding* **1979**, *37*, 1.

(5) Riley, M. J.; Hitchman, M. A.; Reinen, D. *Chem. Phys.* **1986**, *102*, 11.

(6) Samouel, M.; De Kozak, A. *C. R. Acad. Sci., Ser. C* **1969**, *268*, 2312.

0020-1669/90/1329-2123$02.50/0

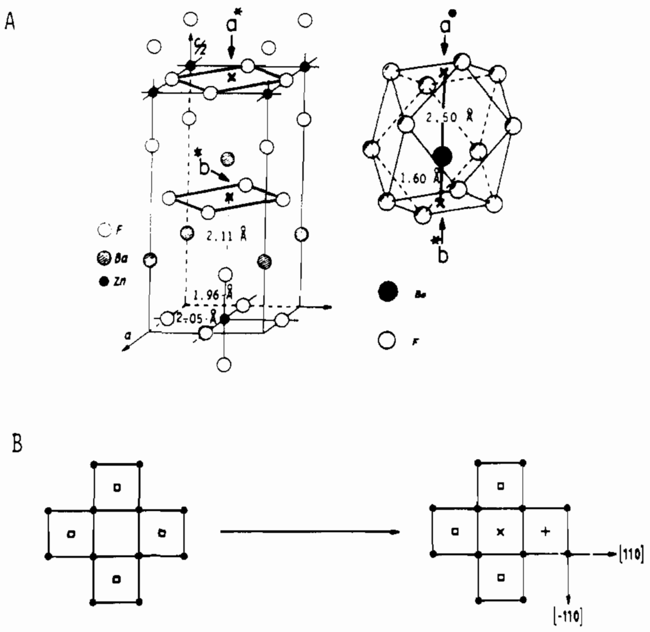

Figure 1. (A) Unit cell of Ba_2ZnF_6 and coordination polyhedron of Ba^{2+}. Possible positions of Cu^{2+} (center II) are additionally marked (a^*, b^*). Reprinted with permission from ref 2. Copyright 1967 Barth. (B) Position of Cu^{2+} (Centre II) in the plane of corner-connected ZnF_6 octahedra: (+) Zn^{2+} vacancy; (×) interstitial Cu^{2+}.

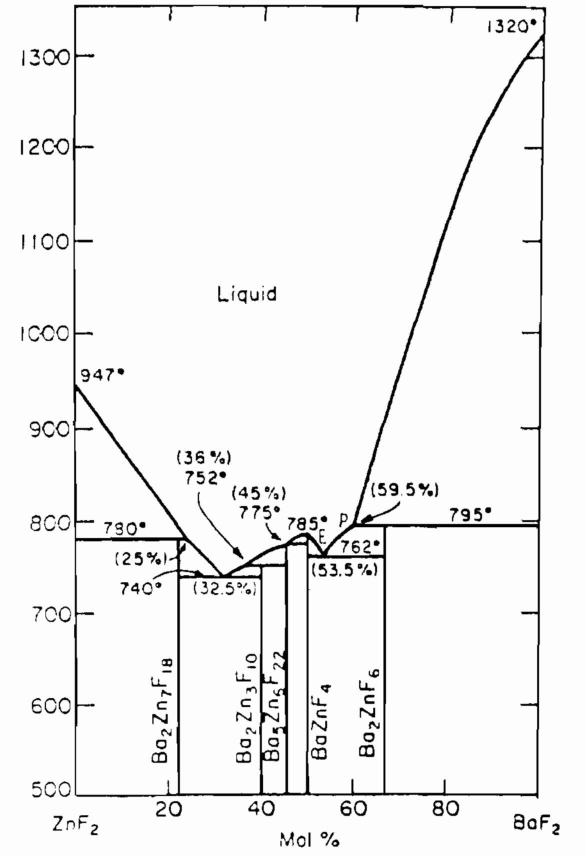

Figure 2. Phase diagram for BaF_2–ZnF_2. *P* and *E* denote the peritectic and eutectic points mentioned in the text. Reprinted with permission from ref 6. Copyright 1969 CDR-Centrale des Revues.

mbar) in order to reduce the oxygen content to a minimum. Vacuum conditions could be used without changing the stoichiometry because at the growth temperature of 805 °C there was no noticeable evaporation of one of the fluoride components. The heating and cooling rates were 25 and 5 °C/h, respectively. The products obtained by this method had a cylindrical shape and consisted in the lower part of pure transparent crystallized Ba_2ZnF_6 and in the upper part of a eutectic composition. The Ba_2ZnF_6 part consisted of small single crystals of 40–400 mm³ size. X-ray diffraction analysis confirmed the formation of Ba_2ZnF_6. Ba_2ZnF_6 crystals, doped with 0.5–5.0 mol % CuF_2, were grown with an optimized crucible lowering rate of 0.28 mm/h. The procedure resulted in Cu-doped Ba_2ZnF_6 crystals of good quality and homogeneity. They showed a weak blue-green color with a distinct pleochroism and a yellow-green luminescence at $\lambda = 555$ nm (UV-excitation: $\lambda = 313$ nm). Lower growth rates as 0.28 mm/h as well as Cu concentrations of about 5 mol % have led to inclusions of metallic copper in the surface regions due to the reducing growth conditions, which do not exclude the formation of Cu(0) or Cu(I). Most of the Cu dopant is in the (+II) oxidation state, however.

B. Spectroscopic Measurements. ENDOR Investigation. In an electron nuclear double resonance (ENDOR) experiment, nuclear magnetic resonance (NMR) transitions of neighbor nuclei of a paramagnetic center are detected via the intensity of a simultaneously induced slightly saturated EPR transition. The intensity of the EPR increases by about 1% when nuclear transitions are induced by a suitable radio frequency (rf) magnetic field. Thus it is possible to combine the high resolution power of NMR with the relatively high sensitivity of EPR.[7] ENDOR experiments were performed in an X-band custom-built computer-controlled EPR/ENDOR spectrometer by using the stationary ENDOR method.[8,9] For the ENDOR experiments, a microwave power of about 0.5 mW was applied to a cylindrical TE_{011} cavity with a loaded Q of about 10.000. The rf was chopped with a frequency of 1 KHz, and the change of the EPR absorption (the ENDOR signal) was detected by using an ordinary lock-in technique. ENDOR spectra were measured in the frequency range from 10 to 160 MHz at a temperature of 4 K. In order to determine the anisotropy of the ligand hyperfine interactions, the sample was rotated in the (001) and the (010) or (100) crystal planes, and an ENDOR spectrum was taken for each angle step using 0.5° increments. Special software algorithms were used to process the data and to obtain the angular dependence of the hyperfine and ligand hyperfine interactions.[9]

EPR Investigation. EPR measurements have been carried out with a Varian E-15 spectrometer operating at X-band ($\nu \approx 9.4$ GHz) and Q-band frequencies ($\nu \approx 35$ GHz) at 298, ≈130, 77, and 4.2 K. X-band measurements were performed between 4.2 and 298 K by using an Oxford Instruments liquid-helium flow cryostat. DPPH was used as internal standard ($g = 2.0036$). Crystal slabs, which were polished parallel and perpendicular to a grown (001) face, were used for the measurement of the angular dependencies of the **g** and hyperfine tensors. For adjustment purposes, the crystal was located on the flat side of a quartz rod and on the face of a LiF cube in case of X- and Q-band frequencies, respectively. Uncertainties are estimated to be ±0.002 for the g values and to $\pm 2 \times 10^{-4}$ cm^{-1} for the A components—unless stated otherwise.

III. EPR Results

The angular dependencies of the g values of the two different centers in the three mutually perpendicular planes (001) and (010) or (100) are depicted in Figure 3. The symmetry axes of both centers clearly align with the c crystal axis. While the **g** tensor of center I is axially symmetric with respect to the c axis of the tetragonal unit cell, there may be a slight deviation from axial symmetry for center II, which will be discussed below. Center I corresponds to Cu^{2+} in the tetragonally compressed F^- octahedron of the regular Zn^{2+} site. The low-temperature g values (4.2 K), $g_\parallel = 1.99_2$ and $g_\perp = 2.36_7$ ($g_{av} \simeq 2.24$), are indicative of a essentially pure d_{z^2} ground state (see Discussion) and are very similar to those already reported for powder samples.[1] The **g** tensor is distinctly temperature-dependent, with an increase of $g_\parallel$ and a decrease of $g_\perp$, as the temperature is raised (Figure 4). We explain this behavior by an admixture of $d_{x^2-y^2}$ into the d_{z^2} ground state (see Section V).

Center II is clearly due to Cu^{2+} with a $d_{x^2-y^2}$ ground state. The g values (4.2 K), $g_\parallel = 2.43_2$ and $g_\perp = 2.07_6$ ($g_{av} \simeq 2.19_5$), are not significantly temperature dependent.

Center I. The $g_\parallel$ signal shows a reasonably well-resolved hyperfine structure at lower temperatures (Figure 5), which is caused by the interactions with the Cu^{2+} ($I = {}^3/_2$) and the six F^- ($I = {}^1/_2$) nuclei. Computer simulations suggest the values $|A_\parallel(\mathrm{Cu})| = 126$ (2), $|A_z(2\mathrm{F}(1))| = 137$ (2), and $|A_{y'}(4\mathrm{F}(2))| = 15$ (2) (in

---

(7) Feher, G. *Phys. Rev.* **1956**, *103*, 834.

(8) Niklas, J. R. Habilitationsschrift, Uninversität-Gesamthochschule Paderborn, 1984. Seidel, H. Habilitationsschrift, Universität Stuttgart, 1966.

(9) Niklas, J. R. *Radiat. Eff.* **1983**, *72*, 39.

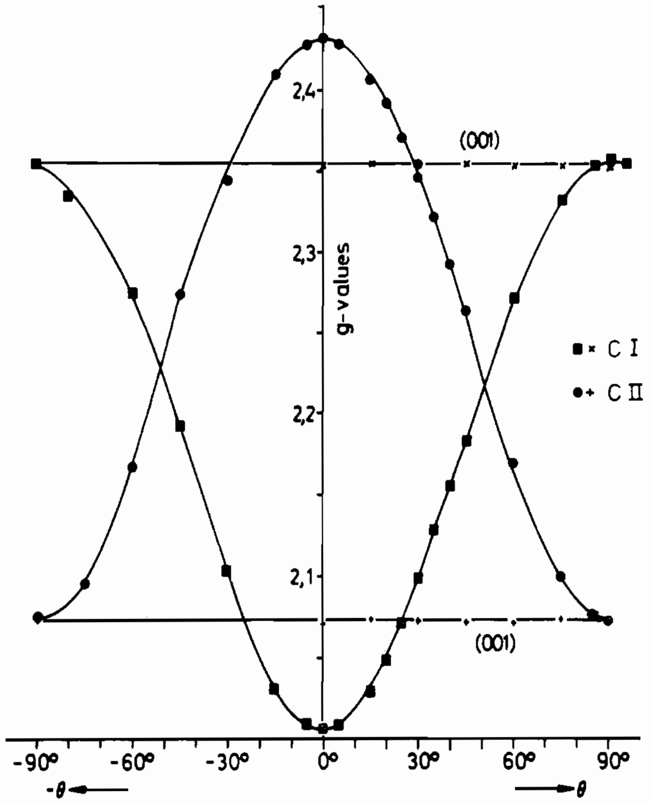

Figure 3. Angular dependence of the g values for centers I and II at 298 K and 35 GHz with the magnetic field rotated in the (001) and (010) or (100) plane.

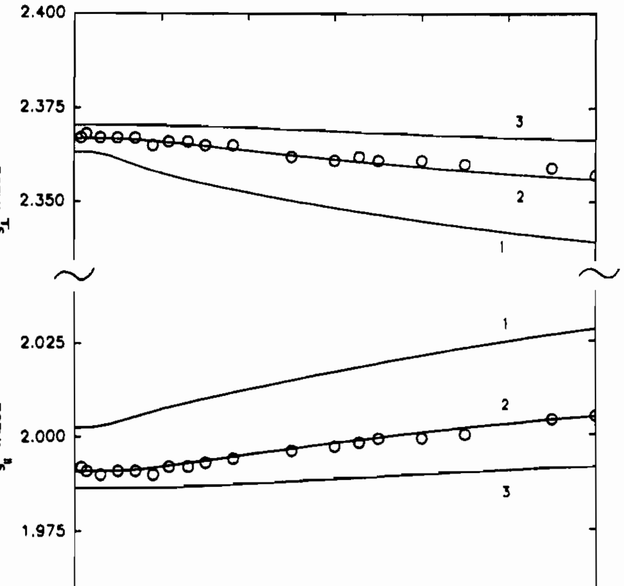

Figure 4. Temperature dependence observed for $g_\parallel$ and $g_\perp$ of center I (circles). The variation of the g values calculated by the method outlined in Section V are shown as full lines. Parameters values A_1 = 673 cm^{-1}, $h\nu$ = 220 cm^{-1}, and β = 80 cm^{-1} were used, with the axial strain parameter being set at S_θ = −500, −1000 and −2000 cm^{-1} for curves 1–3, respectively (see also Figure 11 B–D).

Table I. Fluoride and Copper Hyperfine Parameters (cm^{-1} × 10^{-4}) for Centers I (4.2 K) and II (298 K) in Copper-Doped Ba_2ZnF_6 Estimated from the EPR Spectra, with Values for K_2ZnF_4:Cu (Center I; 4.2 K) Given in Parentheses (cm^{-1} × 10^{-4})

atom	A	center I	center II
F(1)	$A_{x'y'}$	a (26)	
F(2)		15 (14)	38[c]
F(1)	$A_{z'}$	139 (133)	
F(2)		a (49)	139
Cu	$A_\parallel$	126 (76)	−148
	$A_\perp$	22[b] (−30)	−13, −17

[a] Not resolved. [b] Estimated value. [c] Assuming $A_{x'} \simeq A_{y'}$.

units of 10^{-4} cm^{-1}, 4.2 K data, uncertainty width in parentheses), with the fluoride hyperfine parameters based on the coordinate system of Figure 6. The two former values match with those derived earlier from powder values.[1] The four-line fine structure of the $g_\parallel$ signal with two less intense satellites at higher and lower magnetic fields is explained by the assumption of nearly equal $|A_\parallel(\mathrm{Cu})|$ and $|A_{z'}(2\mathrm{F}(1))|$ values. As $|A_\parallel(\mathrm{Cu})|$ decreases with increasing temperature, $|A_{z'}(2\mathrm{F}(1))|$ also becomes slightly smaller (Figure 7). Both variations may be explained by a $d_{x^2-y^2}$ admixture to the ground state that increases as the temperature rises (see Discussion). The expected rather small interaction with the equatorial F(2) ligands is nicely resolved at temperatures ≲90 k by imposing a quintet hyperfine structure on each line (Figure 5B).

Unfortunately $g_\perp$ ((001) plane) is not resolved in hyperfine structure components at all (Figure 8). This situation is different from that of Cu^{2+}-doped K_2ZnF_4, where hyperfine constants $|A_\perp(\mathrm{Cu})|$, $|A_{z'}(2\mathrm{F}(2))|$, $|A_{y'}(2\mathrm{F}(1))|$, and $|A_{x'}(2\mathrm{F}(2))|$ could be evaluated from computer simulations (Table I).[10] However, in the case of Cu^{2+}-doped Ba_2ZnF_6, lower values are expected for some of these parameters. In particular $A_\perp$(Cu) is estimated to be only 22 × 10^{-4} cm^{-1} and also $|A_{z'}(2\mathrm{F}(2))|$ should be smaller than 49 × 10^{-4} cm^{-1} (see Section VI), because almost no $d_{x^2-y^2}$ admixture occurs at 4.2 K (in contrast to the mixing coefficient of 0.2 for Cu^{2+} in K_2ZnF_4).[5] This is because the tetragonal compression of the CuF_6 polyhedra is more pronounced in Ba_2ZnF_6 and the transfer of unpaired spin density to the in-plane fluoride ligands is reduced in comparison to that of Cu^{2+}-doped K_2ZnF_4.

The cause of the relatively poor resolution of the spectra of center I compared with those of center II (see below) is not readily apparent. Interactions between the paramagnetic species do not seem to be important, as broad signals were also observed for crystals containing very small concentrations of Cu^{2+}. Possibly, inhomogeneous crystal strain effects are the dominant cause of the broadening. If these largely affect the orientation or bond distances of the axial fluorides, they would have little effect on the center II complex, assuming this to be the planar CuF_4^{2-} species.

Center II. The quartet structure of the $g_\parallel$ signal (298 K) due to $A_\parallel$(Cu) = −148 (2) × 10^{-4} cm^{-1} is superimposed by (partly overlapping) quintets caused by the superhyperfine interaction with four equatorial F(2) ligands: $|A_{y'}(4\mathrm{F}(2))|$ = 41 (2) × 10^{-4} cm^{-1} (Figure 5). A rather good agreement of the simulated with the experimental spectrum is obtained on the basis of these values.

In the (001) plane a nicely resolved quintet signal is observed in the [110] (or [$\bar{1}$10]) direction (Figure 8B). The splitting is obviously due to the interaction with the four equatorial ligands that are equivalent in this orientation ($A_{\mathrm{eff}}(4\mathrm{F}(2))$ = 104 (2) × 10^{-4} cm^{-1}). Each quintet line is further split by the interaction with the copper nucleus. However, the structure associated with this interaction exhibits translational symmetry, as expected for the superposition of two equivalent sets of lines separated by a small magnetic field (≈5 × 10^{-4} T), rather than the inversion symmetry expected for a single set of EPR lines (Figures 8C). This separation corresponds to a very small in-plane g anisotropy, which may be caused by neighboring Zn^{2+} vacancies in the lattice along the [110] or [$\bar{1}$10] directions (Figure 1). The optimum simulation was obtained if a small anisotropy of the in-plane copper(II) hyperfine values was also assumed (Table I). The signals in the [100] and [010] directions are equivalent and consist of a triplet as a result of the interaction with two F(2) ligands along z'. Each triplet is split again into a triplet due to the two F(2) ligands along x' (Figure 8A). The spectra in the (001) plane

---

[10] Hitchman, M. A.; McDonald, R. G.; Reinen, D. *Inorg. Chem.* **1986**, *25*, 519.

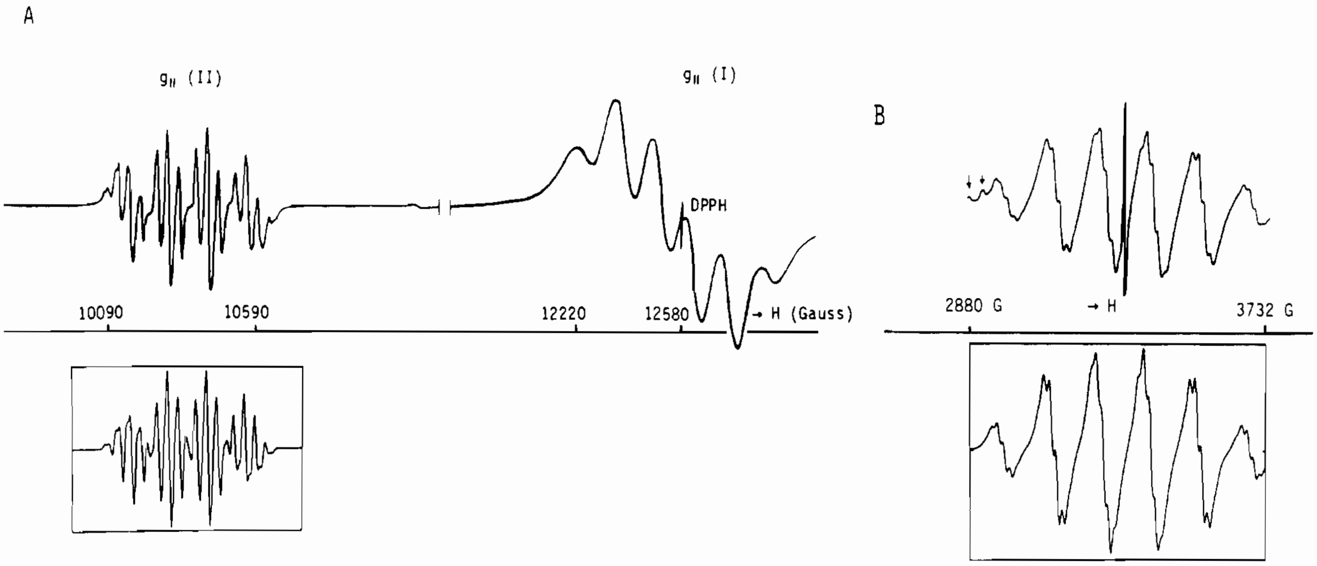

Figure 5. Single-crystal EPR spectra with the magnetic field parallel to the [001] direction: (A) Q-band spectrum at 298 K (above) and simulated $g_\parallel$ signal of center II (below) [ΔH range = 790 G; $|A_\parallel(\mathrm{Cu})| = 148 \times 10^{-4}$ cm^{-1}; $|A_{x'y'}(4\mathrm{F}(2))| = 38 \times 10^{-4}$ cm^{-1}.] (B) X-band spectrum of center I at 60 K (above) with simulation (below) [ΔH range = 850 G; $|A_\parallel(\mathrm{Cu})| = 126 \times 10^{-4}$ cm^{-1}; $|A_{z'}(2\mathrm{F}(1))| = 139 \times 10^{-4}$ cm^{-1}; $|A_{y'}(4\mathrm{F}(2))| = 16 \times 10^{-4}$ cm^{-1}.] (The first two peaks in the low-field region are due to a partial overlap with center II.)

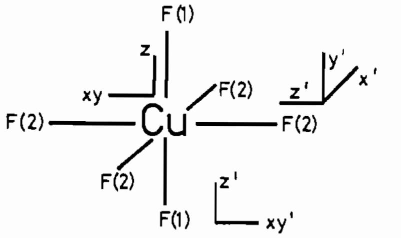

Figure 6. Coordinate system used to define the copper (unprimed) and fluoride (primed) hyperfine tensors. The fluoride z' axes are always pointing to Cu. For center II, the fluoride F(1) is absent.

can be simulated reasonably well with the parameter set: $|A_{z'}(2\mathrm{F}(2))| = 139\ (2) \times 10^{-4}$, $|A_{x'}(2\mathrm{F}(2))| = 35\ (2) \times 10^{-4}$, and $|A_\perp(\mathrm{Cu})| = 15\ (2) \times 10^{-4}$ cm^{-1}. The fluoride hyperfine values (Table I) are consistent with those observed in the directions deviating from the Cu–F bonds by $\varphi = 45°$ [$A_{\mathrm{eff}}(4\mathrm{F}(2)) = 1/2^{1/2}[(A_{z'}(2\mathrm{F}(2)))^2 + (A_{x'}(2(\mathrm{F}(2)))^2]^{1/2} = 101 \times 10^{-4}$ cm^{-1}] and also with those derived from ENDOR spectroscopy.

IV. ENDOR Results

Center I. In order to observe ENDOR signals a sufficient saturation of the EPR signal must be achieved without too high a microwave power being applied to the microwave cavity (≤ 1 mW).[11] This was impossible for center I even at the lowest available temperature of 3.5 K. Dynamic effects may be responsible for the short electronic relaxation time T_1, but also spin–spin interactions between the Cu^{2+} centers due to clustering, which are well-known to significantly lower T_1, cannot be excluded as a possible reason.

Center II. The electronic relaxation time T_1 for this center was considerably larger than that for center I, enabling successful ENDOR experiments. It was the main purpose of these experiments to clarify the lattice position of Cu^{2+} and to gain additional information about the electronic structure of this defect. In the first experiment, the static magnetic field was rotated in the (001) plane of the crystal. The angular dependence of the fluoride ligand hyperfine interactions is shown in Figure 9. This is described by the spin Hamiltonian in (1),[11] where the symbols have the following meaning: g_e, electron g factor; μ_B, Bohr magneton; $\vec{B}_0$, static magnetic field; $\vec{S}$, electron spin operator, $\vec{I}$, nuclear spin operator; A, ligand hyperfine interaction tensor; g_i, nuclear g value; μ_i, nuclear magneton.

$$H = g_e\mu_B\vec{B}_0\vec{S} + \sum_{k=1}^{4}(\vec{I}_kA_k\vec{S} - g_i\mu_i\vec{B}_0\vec{I}_k) \qquad (1)$$

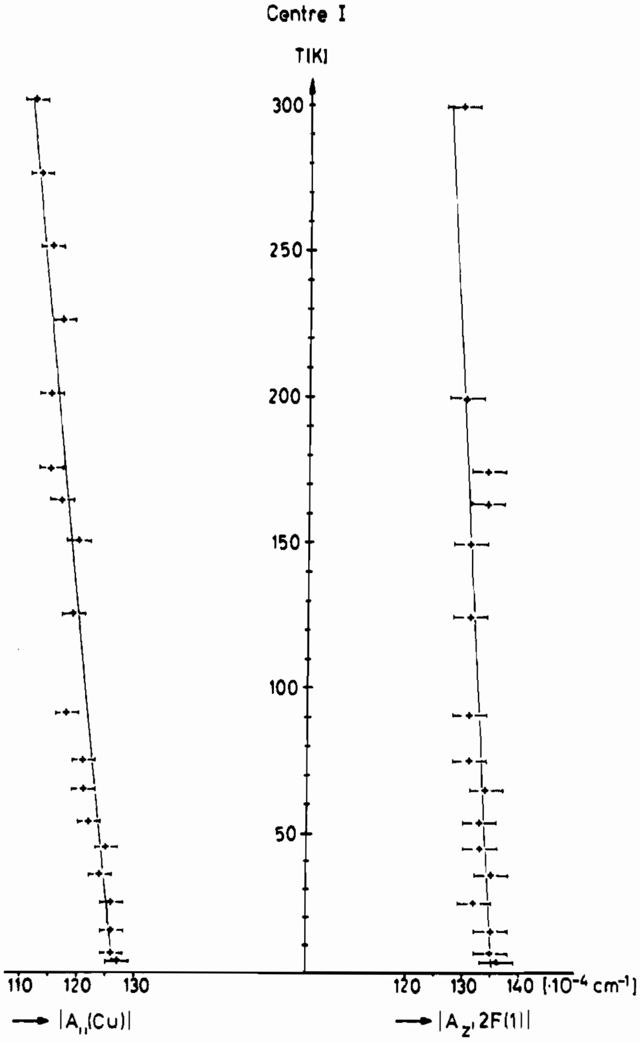

Figure 7. Temperature dependence of $|A_\parallel(\mathrm{Cu})|$ (left) and $|A_{z'}(2\mathrm{F}(1))|$ (right) for center I.

---

(11) Schweiger, A. *Struct. Bonding* **1982**, *51*, 1.

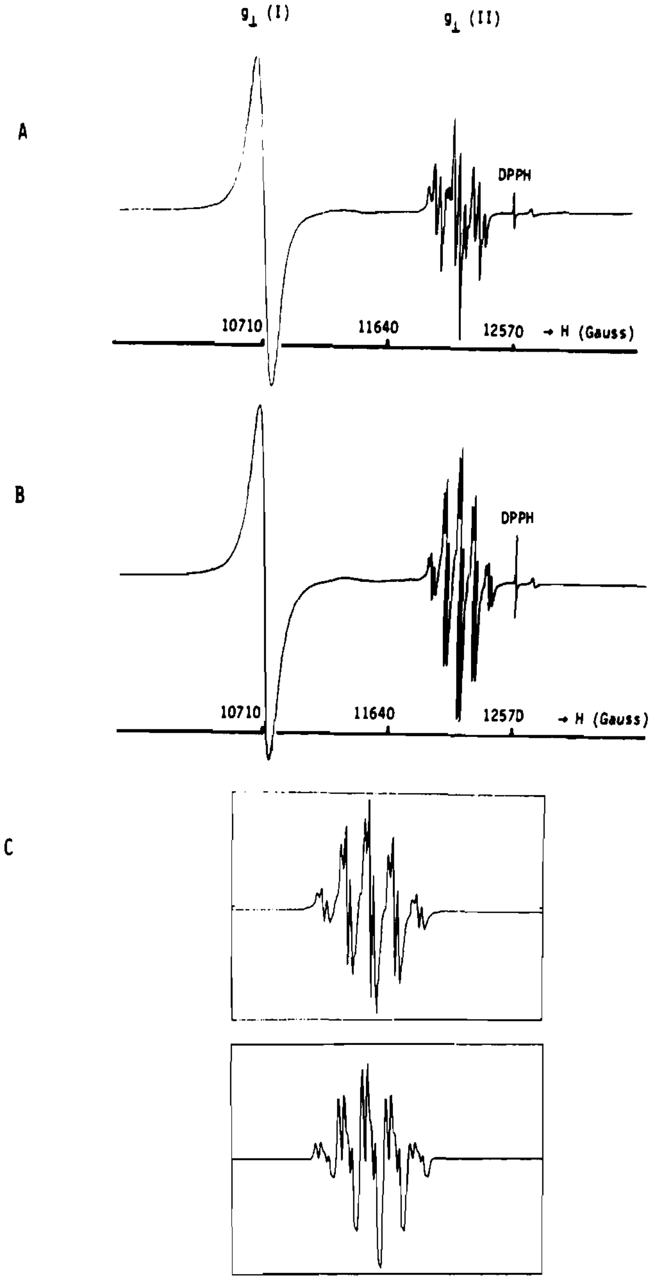

Figure 8. Single-crystal EPR spectra (35 GHz, 298 K) with the magnetic field parallel to [100] or {010} (A) and parallel to {110} (B). The experimental $g_\perp$ signal of center II in the [110] direction (above) is shown together with the simulated spectrum (below) [ΔH range = 1400 G; $|A_y(2F(2))| = 139 \times 10^{-4}$ cm^{-1}; $|A_x(2F(2))| = 35 \times 10^{-4}$ cm^{-1}; $|A_\perp(\mathrm{Cu})| = 13$ and 17×10^{-4} cm^{-1}] in part C. A tiny anisotropy of 0.001 in $g_\perp$ was assumed in the simulation (see text).

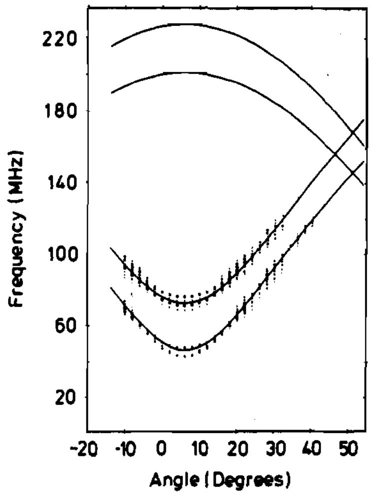

Figure 9. Angular dependence of ENDOR lines for rotation of the magnetic field in the (001) plane [dots, experimental points (+8° corresponds to the magnetic field parallel to {001] or {010]); full lines, curves calculated by fitting of free parameters—see text].

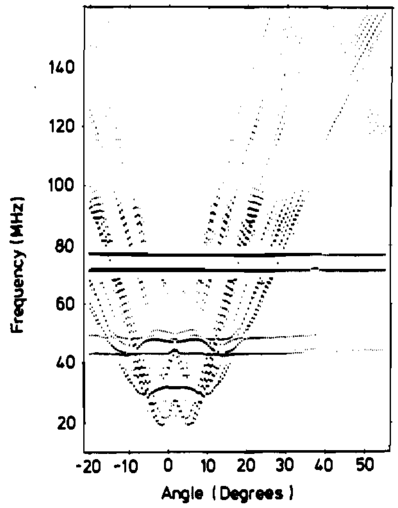

Figure 10. Angular dependence of ENDOR lines for rotation of the magnetic field in the (100) or (010) plane (+2° corresponds to the magnetic field perpendicular to the *c* axis).

In a simple first order solution of (1), ENDOR lines are observed at frequencies, f_{ENDOR}, given by

$$f_{\mathrm{ENDOR}} = 1/h|m_s W_{\mathrm{lhf}} - g_i\mu_i\vec{B}_0| \tag{2}$$

where h is Planck's constant, m_s the electronic quantum number, and W_{lhf} the ligand hyperfine interaction energy, which depends on the A_k tensor components. The full bent lines in Figure 9 correspond to calculated values of (1), assuming the interaction of Cu^{++} with four fluoride ions in a square-planar geometry. This was verified by measuring the positions of the ENDOR lines, f_{ENDOR}, as a function of the magnetic field, which indeed yields the nuclear g_i value for fluorine according to eq 2. In Figure 9 there are two sets of almost parallel bent lines. The lines of each set correspond to the values $m_s = +^1/_2$ and $m_s = -^1/_2$ according to eq 2, in correspondence with an electron spin of $S = {}^1/_2$. The small splittings of the experimental ENDOR, which are not taken in account by the calculation are due to second order effects in the spin Hamiltonian (eq 1) rather than to a deviation from an exact square-planar arrangement of the fluoride ligands. These reflect the strong interaction with those two fluoride ligands which lie in the magnetic field direction and give rise to the calculated upper ENDOR lines in Figure 9. Though there is no noticeable *direct* coupling between different nuclear spins, the strong interaction between the electron and a nuclear spin modifies the electronic wave function, leading to a line splitting for the interaction with a different nucleus. This mechanism is termed "indirect coupling" between nuclear spins.

From the symmetry of the lines in Figure 9, it is apparent that the Cu^{2+} must reside on the [001] vector, which passes through the center of the unit cell sketched in Figure 1. Its exact position on this line was determined by an additional ENDOR experiment, where the magnetic field was rotated in the (100) or (010) plane (Figure 10). The two straight lines between 70 and 80 MHz are due to the interaction with the two fluoride ligands whose bond directions with respect to Cu^{2+} are perpendicular to the plane of magnetic field rotation. The observed two lines for this interaction again reflect the same indirect coupling effect discussed for Figure 9. The fact that these lines exhibit no angular dependence (except for very small second-order effects) provides clear evidence that Cu^{2+} resides exactly on a mirror plane of the crystal perpendicular to the *c* axis. Again, there is no evidence for a distortion of the square-planar symmetry of the four fluoride ions around Cu^{2+}. The strongly angular dependent ENDOR resonances represented by the dots in Figure 10 correspond to the hyperfine interaction with the Cu nucleus. This angular dependence is rather complex because of the presence of two Cu isotopes, the quadrupole interaction due to the nuclear spin $I = {}^3/_2$ for both Cu isotopes, and indirect nuclear couplings with the fluoride ligands. Around 0°, it can be described qualitatively by the simple first-order equation (2). Because the frequency in eq 2 occurs as an absolute magnitude, parts of the angular dependence that would correspond to negative frequency values are folded back at the zero frequency line. A diagonalization of the spin Hamiltonian including, in addition to the effects described by eq 1, the dipolar and quadrupolar interaction with the Cu nucleus exactly reflects the experimentally observed behaviour of the ENDOR lines.

The interaction constants for the nearest-neighbor fluoride nuclei and the Cu nucleus obtained with ENDOR are identical with those obtained from the analysis of the EPR spectra. Lines due to interactions with nuclei further away from the center are not found in the ENDOR spectra. Their interaction constants must therefore be smaller by about 2 orders of magnitude compared with those for the analyzed interactions.

V. Temperature Dependence of the *g* Values of Center I and the Ground-State Potential Surface

As the temperature is raised from 4 to 290 K, the principal *g* values of center I tend to converge (Figure 4). The effect is very similar to that reported recently[5,10] for the analogous CuF_6^{4-} complex present in Cu^{2+}-doped K_2ZnF_4, and to that observed[12] for the centers $Cu(NH_3)_2Cl_4^{2-}$ and $Cu(NH_3)(H_2O)Cl_4^{2-}$ formed when Cu^{2+} is doped into NH_4Cl. The unusual behavior of these systems is thought to be due to the vibronic admixture of a small proportion of $d_{x^2-y^2}$ orbital into the predominantly d_{z^2} ground state. A theoretical model has been developed that satisfactortly explains the temperature dependence of the g tensors of these complexes, and we report here the application of this approach to center I of Cu^{2+}-doped Ba_2ZnF_6. The methodology of the calculations follows the procedure described previously.[5,12,13] Basically, the method involves calculating the *g* values from the vibronic wave functions which are solutions to a vibronic Hamiltonian perturbed by a strain caused by the inequivalence of the fluoride ligands. The overall molecular *g* values at any temperature are obtained from the weighted average of the *g* values of the individual vibronic energy levels as given by the Boltzmann population distribution. It is assumed that there is rapid exchange between the thermally populated vibronic levels on the time scale of the EPR experiment. The vibronic Hamiltonian is that of the usual Jahn–Teller coupling, H_{JT}, with the addition of terms representing the strain, H_{ST}. The approximation is made that the strain term does not destroy the symmetry of the cubic part of the Hamiltonian, which takes the general form[5,10]

$$
\begin{gathered}
H = H_0 + H_{JT} + H_{ST} \\
H_0 = [0.5h\nu(P_\theta^2 + P_\epsilon^2 + Q_\theta^2 + Q_\epsilon^2) + K_3 Q_\theta(Q_\theta^2 - 3Q_\epsilon^2)]I \\
H_{JT} = A_1(Q_\theta\sigma_z - Q_\epsilon\sigma_x) + A_2[(Q_\theta^2 - Q_\epsilon^2)\sigma_z + 2Q_\theta Q_\epsilon\sigma_x] \\
H_{ST} = S_\theta\sigma_z - S_\epsilon\sigma_x
\end{gathered}
\tag{3}
$$

where A_1, A_2, and K_3 are the first- and second-order coupling constants and the cubic anharmonicity of the tetragonal component of the Jahn–Teller active ϵ_g vibration Q_θ, respectively, and σ_x, σ_y, and I are defined in eq 4. The energy of the ϵ_g vibration would

$$
\sigma_x = \begin{bmatrix} 0 & 1 \\ 1 & 0 \end{bmatrix} \quad \sigma_z = \begin{bmatrix} 1 & 0 \\ 0 & -1 \end{bmatrix} \quad I = \begin{bmatrix} 1 & 0 \\ 0 & 1 \end{bmatrix} \tag{4}
$$

be $h\nu$ in the complete absence of the Jahn–Teller effect, and S_θ and S_ϵ are the tetragonal and orthorhombic components of the strain, respectively. All parameters in eq 3 are in units of cm^{-1}.

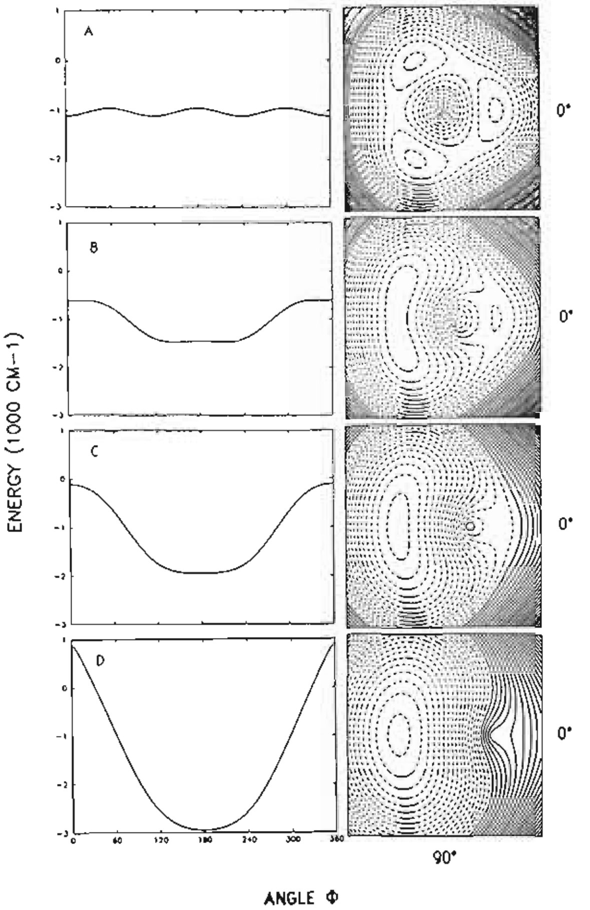

Figure 11. Left-hand side: Circular cross sections of the Mexican hat potential surface along the angular coordinate at the radius ρ_0 $(=A_1/h\nu)$. Right-hand side: Contour plots of the lower adiabatic surfaces. The contour interval is 40 cm^{-1}, and negative energies are shown as dashed lines. Parameter values $A_1 = 673$ cm^{-1}, $h\nu = 220$ cm^{-1}, and $\beta = 80$ cm^{-1} were used in each calculation, with the axial strain parameter being set at $S_\theta = 0$, −500, −1000, and −2000 cm^{-1} for plots A–D, respectively.

The desired energy levels and wave functions of the CuF_6^{4-} complex are obtained by diagonalizing the matrix formed by applying Hamiltonian (3) to a truncated set of vibronic basis functions. This basis consisted of the two e_g ($d_{x^2-y^2}$, d_{z^2}) metal orbital wave functions and the N $[={}^1/_2(n_y + 1)(n_y + 2)]$ two-dimensional harmonic oscillator wave functions of the ϵ_g vibration up to the level n_y. Because of the strong coupling, the linear displacement ρ is large, and a sizable basis set of vibrational wave functions is needed. In the present calculations a value of $n_y = 30$, corresponding to a basis size of $N = 992$, was found to provide a satisfactory convergence (this was tested by monitoring the effect of varying the basis size). Due to the large size of these matrices, a diagonalization routine was adopted that incorporated condensed storage techniques by using the Lanczos algorithm.[14] Neglecting the kinetic energy terms, in the absence of lattice strain, vibrational anharmonicity, and second-order coupling, the adiabatic potential described by the above equation takes the form of the well-known "Mexican Hat" surface. Here the potential energy minimum has the form of a circular well, with a substantial radial displacement in the ϵ_g mode ρ, but no dependence on ϕ, ie. with the two components Q_θ and Q_ϵ remaining equivalent:

$$
Q_\theta = \rho\cos\phi \qquad Q_\epsilon = \rho\sin\phi \tag{5}
$$

The second-order electronic and anharmonic terms discriminate between Q_θ and Q_ϵ, and hence produce the "warped" Mexican hat potential surface, with energy minima occurring at $\phi = 0$, 120, and 240° for $A_2 > 0$. They correspond to tetragonal elongations

---

(12) Riley, M. J.; Hitchman, M. A.; Reinen, D.; Steffen, G. *Inorg. Chem.* **1988**, *27*, 1924.

(13) Riley, M. J.; Hitchman, M. A.; Wan Mohammed, A. *J. Chem. Phys.* **1987**, *87*, 3766.

(14) O'Brien, M. C. M.; Evangelou, S. N. *J. Phys. C.* **1980**, *13*, 611.

of the ligands along z, x, and y, while the three saddle points at ϕ = 60, 180, and 300° correspond to tetragonal compressions. The "rim" of such a Mexican hat potential surface is shown on the left side of Figure 11A, while the corresponding energy contour plot is shown on the right side of this figure. Because of the cubic dependence on ρ, the inclusion of the anharmonicity parameter K_3 in the calculations causes computational problems when, as in the present case, the displacement in ρ is large.[15] Although it is more likely that the cause of the warping is in fact anharmonicity, probably supplemented by configuration interaction between the metal a_{1g} (d_{z^2}) and a_{1g} (4s) orbitals,[16] the correct form of the potential surface may be represented quite satisfactorily by using just the parameter A_2,[12,13] and for the sake of simplicity, this procedure was adopted in the present calculations.

Parameters Used in the Calculations. The values chosen for the linear coupling coefficient and the energy of the Jahn–Teller active ϵ_g vibration were those used previously[5] for the analogous CuF_6^{4-} complex in Cu^{2+}-doped K_2ZnF_4, A_1 = 673 cm^{-1} and $h\nu$ = 220 cm^{-1}. The symmetry of the problem is such that only the tetragonal component of the strain is nonzero. It may be estimated from the energy of the optical transition to the upper Jahn–Teller surface, as given by

$$\Delta E \approx 4E_{JT} + 2|S_\theta| \qquad (6)$$

where the Jahn–Teller stabilization energy is $E_{JT} \approx A_1^2/(2h\nu)$. This transition occurs at ≈ 6300 cm^{-1} for center I,[1,17] which implies a value of $S_\theta \approx -1090$ cm^{-1}, the negative sign indicating an axial compression of the ligand field.

The barrier height 2β between the wells of the warped Mexican hat potential surface in the absence of the strain interaction (Figure 11A) is related to the second-order coupling coefficient by the expression

$$\beta \approx A_2(A_1/(h\nu))^2 \qquad (7)$$

This parameter is generally difficult to estimate.[16] Values between $\beta \approx 50$ cm^{-1} and $\beta \approx 200$ cm^{-1} have been reported recently for a range of copper(II) complexes[1,12,13] and were also explored in the present calculations.

The procedure used to calculate the g values involves estimating the admixture of excited electronic states by spin–orbit coupling.[10] A value of λ = 830 cm^{-1} was used for the spin–orbit coupling constant, and the excited state energies, $E(xz,yz)$ = 9500 cm^{-1} and $E(xy)$ = 12 500 cm^{-1}, were those obtained from the single-crystal polarized electronic spectrum of the center.[17] Covalency effects were accounted for by orbital reduction factors,[18] and optimum agreement with experiment was obtained with $k_\perp$ = 0.86.

Results of the Calculations. Good agreement between the calculated g values and those observed experimentally over the temperature range 4 to 290 K was obtained by using the values S_θ = −1000 cm^{-1} and β = 80 cm^{-1} for the strain and warping parameters, respectively (curves 2 of Figure 4). This value of the strain is identical with a previous estimate based upon the structural parameters of the host lattice[19] and is about twice that deduced[5] for the CuF_6^{4-} center in Cu^{2+}-doped K_2ZnF_4 ($S_\theta \approx -540$ cm^{-1}). Assuming a similar basic Jahn–Teller stabilization energy in the two lattices, the energy of the transition between the lower and upper Jahn–Teller surfaces should shift to higher energy by twice the difference between the strain parameters (eq 6), or ≈900 cm^{-1}, on going from Cu^{2+}-doped K_2ZnF_4 to Ba_2ZnF_6, which agrees quite well with the observed shift of ≈1100 cm^{-1}.[1,19] The increase in magnitude for S_θ deduced for the CuF_6^{4-} center in Ba_2ZnF_6 compared with that in K_2ZnF_4 also agrees well with the structures of the two hosts. Both involve in-plane coordination by bridging ligands and axial coordination by terminal ones. In K_2ZnF_4 all six Zn–F distances are equal within experimental error,[20] so that the strain must be caused exclusively by the stronger σ-bonding power of the terminal fluorides compared with the bridging fluorides. In Ba_2ZnF_6, however, the terminal bonds are significantly shorter than those to the bridging ligands (196 pm compared with 205 pm).[2]

The value of the warping parameter $\beta \approx 80$ cm^{-1} deduced for center I in Ba_2ZnF_6 seems reasonable, falling between that estimated for the similar center in K_2ZnF_4 ($\beta \approx 50$ cm^{-1}),[5] and for the centers $Cu(L)_2Cl_4^{2-}$, L = H_2O or NH_3, formed on doping Cu^{2+} in NH_4Cl ($\beta \approx 100$ cm^{-1}).[12] A considerably higher warping parameter ($\beta \approx 300$ cm^{-1}) has recently been estimated for $Cu(H_2O)_6^{2+}$ in a range of host lattices.[13] It has been suggested[16] that a more pronounced warping of the Mexican hat potential surface is indeed expected for a complex involving isolated ligands compared with a lattice with interconnected polyhedra such as Ba_2ZnF_6.

Potential Surface of Center I. The calculations for Cu^{2+}-doped K_2ZnF_4[5] suggest that the $d_{x^2-y^2}$ orbital contributes only ≈1.9% to the lowest vibronic level. This contribution rises to ≈5.0% for the next level at ≈84 cm^{-1} and ≈6.9% for the following one at ≈178 cm^{-1}, with a progressive increase for still higher levels. The effect on the g values is most pronounced for $g_\parallel$, and even at absolute zero, the $d_{x^2-y^2}$ component causes a slight shift (≈0.01) from the value expected in the absence of vibronic coupling. As the temperature rises above ≈50 K, thermal population of the higher levels causes increasing contamination of the "average" wave function by the $d_{x^2-y^2}$ orbital. Because $g_\parallel$ is much higher for a $d_{x^2-y^2}$ than a d_{z^2} ground state, $g_\parallel$ rises continuously (Figure 4). The reverse is true for $g_\perp$, so that as the temperature rises, $g_\perp$ falls gradually.

As has been discussed in detail elsewhere,[1,4,5,10,12,13,19] the form of the potential surface of a six-coordinate copper(II) complex is strongly influenced by the ratio of the warping parameter to the strain parameter. The former is a measure of the tendency of the Cu^{2+} ion to adopt an elongated tetragonal geometry. If the effect of the strain is to oppose this, which occurs when the axial ligands produce a stronger σ-perturbation than the in-plane ligands, a warped potential surface often results, which gives rise to unusual dynamic behavior. As the magnitude of the strain increases from zero to a modest value, −500 cm^{-1}, the familiar three-well warped Mexican hat surface (β = 80 cm^{-1}) distorts, with shallow minima lying between the angular coordinates ϕ = 120° and 240° and describing orthorhombic ligand geometries (Figure 11B). The saddle point at ϕ = 180° between the minima is only a few wavenumbers high, well below the lowest vibronic level, and corresponds to a compressed tetragonal geometry. The ground-state wave function is therefore extensively delocalized to either side of ϕ = 180°, with about 4% $d_{x^2-y^2}$ character. The g values expected for such a surface are pictured in curves 1 of Figure 4. Even at low temperature, these exhibit a significant shift from the values expected in the absence of vibronic coupling, and the deviation increases dramatically as the temperature rises. Behavior of this kind is observed for the center $Cu(H_2O)(NH_3)Cl_4^{2-}$ in NH_4Cl,[12] and also for the CuF_6^{4-} center in K_2ZnF_4, though here it is thought that the value of β is not quite sufficient to produce orthorhombic minima in the potential surface.[5] For larger ratios of β to S_θ, the barrier height may be large enough to allow localization of the lowest vibronic wave functions within each well. Such a situation is thought to occur for the center $Cu(H_2O)_2Cl_4^{2-}$ in Cu^{2+}-doped NH_4Cl[12] with estimated parameters $\beta \simeq 100$ cm^{-1} and $S_\theta \simeq -200$ cm^{-1}. Here, orthorhombic g values are observed at low temperatures, coalescing to produce a tetragonal g tensor as the temperature is raised, allowing thermal population of more delocalized levels.

A strain parameter of −1000 cm^{-1} localizes the surface minimum firmly at a compressed tetragonal geometry (ϕ = 180°), but the potential rises only gently along the angular coordinate (Figure 11C). Behavior of this type has also been noted for the center $Cu(NH_3)_2Cl_4^{2-}$ of Cu^{2+}-doped NH_4Cl.[12]

---

(15) O'Brien, M. C. M. *Vibr. Spectra Struct.* **1981**, *10*, 321.

(16) Deeth, R. J.; Hitchman, M. A. *Inorg. Chem.* **1986**, *25*, 1225.

(17) Stratemeier, H.; Riley, M. J.; Hitchman, M. A.; Reinen, D.; Steffen, G.; Recker, K.; Wallrafen, F.; Matthies, H. To be submitted for publication.

(18) Gerloch, M.; Miller, J. R. *Prog. Inorg. Chem.* **1968**, *10*, 1.

(19) Reinen, D.; Krause, S. *Inorg. Chem.* **1981**, *20*, 2750.

(20) Herdtweck, E.; Babel, D. *Z. Kristallogr.* **1980**, *153*, 189.

When the strain is doubled again, the potential becomes strongly localized at the $\phi = 180°$ minimum with a compressed tetragonal geometry (Figure 11D). The groundstate is d_{z^2}, and the g values are almost independent of temperature (curves 3 of Figure 4).

VI. Discussion of the Hyperfine Parameters

Center II. The copper hyperfine parameters of center II with a $d_{x^2-y^2}$ ground state are described by eq 8. The values of P and

$$\text{ground state MO:}\quad \phi_g = \alpha d_{x^2-y^2} - \alpha' L_{x^2-y^2}$$

$$A_\parallel = P[-\alpha^2(\kappa + 4/7) + 3/7(g_\perp - g_0) + g_\parallel - g_0] \qquad (8)$$

$$A_\perp = P[-\alpha^2(\kappa - 2/7) + 11/14(g_\perp - g_0)]$$

κ for the free Cu^{2+} ion, which are generally used, are 0.036 cm^{-1} and 0.43.[21,22] The best fit α mixing coefficient for adapting the experimental $A_\parallel$ and $A_\perp$ values (Table I) to eq 7 is 0.92_5.

From the fluoride hyperfine structure analysis, we conclude that center II corresponds to a square-planar CuF_4^{2-} entity, possibly with a further remote fluoride environment above and below the plane. Fluoride coordination in the axial directions would not lead to an additional ligand hyperfine structure by covalency effects because of the shape of the $d_{x^2-y^2}$ orbital and because dipolar contributions are expected to be very small ($<10^{-3}$ cm^{-1}).[10] Because the orientation of the CuF_4^{2-} entities corresponds to the xy plane of the ZnF_6^{4-} octahedra (Figure 3), two reasonable interstitial lattice positions for center II exist in the unit cell of Ba_2ZnF_6 (Figure 1). One of these sites (b^*) is very near to a barium ion (1.6 Å), which would imply that Ba^{2+} is formally substituted by Cu^{2+}—a rather unrealistic assumption. The second possible square-planar CuF_4^{2-} center (a^*) is part of the planes that contain the Zn^{2+} ions. In this case the Cu^{II}–Ba^{II} distance (2.5 Å) is large enough to avoid a strong electrostatic repulsion. Indeed the ENDOR investigations indicate a mirror plane perpendicular to the c axis, supporting the assumption that center II corresponds to an interstitial Cu^{2+} ion coupled with an empty Zn^{2+} position as shown in Figure 1B. A small anisotropy with respect to the [110] and [$\bar{1}$10] directions is expected for this site, because the occupancy of neighboring Zn^{2+} sites is irregular. The EPR spectra indeed give evidence for this lower symmetry effect in these directions (see Section III).

From the ligand hyperfine structure, we can estimate the unpaired spin density transfered from Cu^{2+} to the four F(2) ligands. The respective MO is σ-antibonding, as given in eq 8, if one neglects the tiny admixture of d_{xy} and d_{xz}, d_{yz} by spin-orbit coupling. Hence the equations, relating the principal $A(F^-)$ values to the fractional unpaired electron density in the fluoride 2s and $2p_{z'}$ orbitals (f_s and $f_{p\sigma}$), are rather simple:[10,23,24]

$$A_{z'} = f_s A_s + 2 f_{p\sigma} A_p + 2A_D$$

$$A_{x'y'} = f_s A_s - f_{p\sigma} A_p - A_D \qquad (9)$$

Here, A_s and A_p are splittings due to unit unpaired spin density in 2s and 2p fluorine orbitals, which are reported to have values of 1.764 and 0.059 cm^{-1},[24] or 1.341 and 0.049 cm^{-1}, respectively, for the fluoride ion.[10,23] A_D is the dipolar splitting and is calculated to have a value of $\simeq 3 \times 10^{-4}$ cm^{-1} for the estimated Cu–F spacing of 1.90 Å.[17] The calculated transferred spin densities f_s and $f_{p\sigma}$ are collected in Table II. The estimate of the total spin density transferred to the four F^- ions of center II ($\simeq$27%) is higher than that transferred to the six F^- ions of the compressed CuF_6^{4-} center in K_2ZnF_4, $\simeq$22%. In particular the spin density delocalized onto the four in-plane ligands of the latter complex is lower by a factor of $\geq$3 (Table II), which agrees with the fact that the electron density of the d_{z^2} orbital along the x and y directions is three times smaller than that of the $d_{x^2-y^2}$ orbital.

Table II. Spin Densities from EPR Ligand Hyperfine Values for Center I (A) and II (C) in Cu^{2+}-Doped Ba_2ZnF_6 and for Center I in Cu^{2+}-Doped K_2ZnF_4[5] (B)

	atom	f_s, %	f_p, %
A	F(1)	[$\approx$0.4][a]	[$\approx$8.0][a]
	F(2)	[$\approx$0.2][a]	[$\approx$1.2][a]
B	F(1)	0.4_5	6.7
	F(2)	0.2	1.8
C	F(2)	0.5_5	6.2

[a] Parameters from tentative choices for $A_{x'y'}(F(1)) = 40 \times 10^{-4}$ cm^{-1} and $A_{z'}(F(2)) = 10 \times 10^{-4}$ cm^{-1} (see text).

The transferred spin densities $f_{p\sigma}$ and f_s correspond to mixing coefficients $\alpha'_{p\sigma} = 0.49_5$ and $\alpha'_s \simeq 0.15$, if the symmetry adapted ligand LCAO $L_{x^2-y^2}$ in eq 8 is specified with respect to the $p_{z'}$ and s ligand orbitals. From these values, one obtains an α coefficient of 0.91_5, utilizing the normalization condition for the ground state MO in eq 8 and tabulated overlap integrals[25] (estimated Cu–F(2) spacings $\simeq$1.88 Å, from $CaCuF_4$[30]), in very good agreement with the value calculated from the Cu^{2+} hyperfine structure.

Center I. The g values at 4.2 K indicate an almost pure d_{z^2} ground state and hence a compressed CuF_6 coordination as a static and not partially dynamically averaged effect:

$$\text{ground state MO:}\quad \phi_g = \alpha\, d_{z^2} - \alpha' L_{z^2}$$

$$A_\parallel = P[-\alpha^2(\kappa - 4/7) - 1/7(g_\perp - g_0)] \qquad (10)$$

$$A_\perp = P[-\alpha^2(\kappa + 2/7) + 15/14(g_\perp - g_0)]$$

We can no longer assume for this center, however, that the isotropic hyperfine constant κ has the characteristic value $\kappa_{3d} = 0.43$,[21,22] because symmetry allows an admixture of the 4s wave function into the $3d_{z^2}$ ground state. The isotropic hyperfine constant κ_{4s} is -5.56,[24] and hence a reduction in the magnitude of κ with respect to κ_{3d} or even a negative value is expected. If the mixing coefficient γ of the 4s orbital in the ground-state MO is small with respect to α, the equations for $A_\parallel$ and $A_\perp$ in eq 10, which are valid for a pure d_{z^2} ground state, may still be used, but with an effective κ deviating from κ_{3d} toward κ_{4s}. Because $A_\perp$ could not be observed, we have calculated κ using the experimental $A_\parallel$(Cu), $g_\parallel$, and $g_\perp$ values (Table I), as well as the α parameter of center II (0.92_5). From eq 11, a mixing coefficient $\gamma \simeq 0.22$

$$\gamma^2 \simeq \alpha^2(\kappa - \kappa_{3d})/\kappa_{4s} \qquad (11)$$

can be estimated from the obtained $\kappa = 0.10$, corresponding to a s character of the ground-state electron of 5.0%. With $\kappa = 0.10$, $A_\perp$(Cu) is calculated (eq 10) to be 22×10^{-4} cm^{-1}, which is not resolved in the EPR spectrum.

Assuming a positive $A_\parallel$ and a negative $A_\perp$ value for the Cu^{2+} center in K_2ZnF_4 (Table I), eq 10 yields $\kappa = 0.27$ and $\alpha = 0.92_5$, which is the same α value as for center II in Ba_2ZnF_6. From eq 11, the 4s admixture to the $3d_{z^2}$ ground state amounts to 2.6% ($\gamma \simeq 0.16$). The α, κ, and γ values given here are different from those reported before,[10] which were based on the assumption of positive $A_\parallel$ and $A_\perp$ parameters. In comparison with the results for Cu^{2+}-doped Ba_2ZnF_6, the choice of a negative $A_\perp$ value for the Cu^{2+} center in K_2ZnF_4 leads to more reasonable and consistent bonding parameters, however. The transferred spin densities[10] (Table II) correspond to mixing coefficients $\alpha'_{p\sigma} = 0.27$, 0.36_5 and $\alpha'_s = 0.09$, 0.09_5 for the equatorial plane and the axial directions, respectively, if the symmetry adapted ligand LCAO L_{z^2} in eq 10 is split with respect to the p and s ligand orbitals and the equatorial and axial bond directions. If the normalization condition for the ground-state MO is applied and tabulated overlap integrals[25] are used for the estimated equatorial (2.10 Å) and axial bond lengths (1.89 Å),[10,19] one obtains from the α' mixing coefficients $\alpha = 0.92$, in perfect agreement with the value derived from the Cu^{2+} hyperfine structure.

---

(21) Abragam, A.; Bleaney, B. *Electron Paramagnetic Resonance of Transition Ions*; Clarendon Press: Oxford, U.K., 1970; Chapter 17.

(22) McGarvey, B. R. ESR of Transition Metal Complexes. In *Transition Metal Chemistry*; Carlin, R. L., Ed.; Marcel Dekker, Inc.: New York, 1966; Vol. 3, p 175. McGarvey, B. R. *J. Phys. Chem.* **1967**, *71*, 51.

(23) Owen, J.; Thornley, J. M. *J. Rep. Prog. Phys.* **1966**, *29*, 675.

(24) Morton, J. R.; Preston, K. F. *J. Magn. Reson.* **1978**, *30*, 577.

(25) Smith, D. W. *J. Chem. Soc. A* **1970**, 3108.

The 4s admixture is about twice as large for center I in Ba_2ZnF_6 than for the analogous center in K_2ZnF_4. Apparently the $3d_{z^2}$–4s interaction is comparatively stronger for Cu^{2+}-doped Ba_2ZnF_4 as a consequence of the more pronounced tetragonal compression of the CuF_6 octahedra. Obviously the larger extent of the tetragonal compression of the ZnF_6 host sites in Ba_2ZnF_6 compared to K_2ZnF_4, respectively, has some interesting and far-reaching consequences.

It is noteworthy that both $A_{\|}$[Cu] and $A_{z'}$[2F(1)] decrease in magnitude as the temperature is raised (Figure 7). In each case, this may be explained in terms of an increase in the $d_{x^2-y^2}$ contribution to the ground-state wave function that accompanies the thermal population of higher vibronic levels of the ground state (see section V). For the metal hyperfine parameter, the decrease is caused by the fact that $A_{\|}$ is expected to be positive for a d_{z^2} groundstate but negative for a $d_{x^2-y^2}$ groundstate. The variation of $A_{z'}$[2F(1)] reflects the decreasing d-electron density of Cu^{2+} in the directions toward the axial ligands with increasing temperature.

Unfortunately the hyperfine splitting of the $g_{\perp}$ signal is not resolved. It was also not possible—as in case of Cu^{2+}-doped K_2ZnF_4—to deduce the relevant $A_{x'y'}$(4F(1)), $A_{z'}$(2F(2)), and $A_{\perp}$(Cu) parameters from the angular dependence in the (100) or (010) planes, due to the presence of the two signals of centers I and II, which overlap in the critical regions. Because the $A_{z'}$(2F(1)) and $A_{x'y'}$(4F(2)) parameters are practically equal in both cases, one may suggest, however, that also the $A_{z'}$(2F(2)) and $A_{x'y'}$(4F(1)) values are not very different. The careful spectral analysis shows that the mentioned parameters should be $\leq 40 \times 10^{-4}$ cm^{-1}. If this value is adopted for $A_{z'}$(2F(2)), estimated equatorial f_s and $f_{p\sigma}$ spin densities of ≈0.2 and ≈1.2%, respectively, result from eq 9 with $A_D \simeq 2.3 \times 10^{-4}$ cm^{-1} [10] (Table II). This reduction of equatorial spin transfer with respect to the Cu^{2+} center in K_2ZnF_4 is expected to be accompanied by correspondingly higher axial spin transfer, in order to produce a total transferred spin density of (at least) 22%, which was found for Cu^{2+}-doped K_2ZnF_4.[10] The choice of a $A_{x'y'}$(4F(1)) value of 10×10^{-4} cm^{-1} yields $f_s \approx 0.4\%$ and $f_{p\sigma} \approx 8.0\%$ for the axial directions (eq 9 with $A_D \simeq 2.8 \times 10^{-4}$ cm^{-1})[10] is in agreement with this assumption. The ratio between the suggested axial and equatorial spin transfer, which should be 2 for a pure d_{z^2} ground state and equal axial and equatorial bond lengths, seems to be larger (≈ 3) than for Cu^{2+}-doped K_2ZnF_4 (1.8). This trend is expected, because in case of center I in Ba_2ZnF_6 the $d_{x^2-y^2}$ admixture to the ground state vibronic wavefunction is negligible and the axial compression and equatorial bond extension more pronounced than for the CuF_6 polyhedron in K_2ZnF_4.[17] In conclusion, one may state that the transferred spin densities and mixing coefficients are similar for center I in K_2ZnF_4 and Ba_2ZnF_6, presumably with a relatively more pronounced covalency in the *z* direction with respect to the *xy* plane in the latter case.

General Discussion. The transferred spin density in $Ni^{II}F_6$ polyhedra is reported to be $\approx 16._5\%$[22] and hence lower by a factor of about 1.5 than the corresponding magnitudes for the analyzed square-planar $Cu^{II}F_4$ and tetragonally compressed $Cu^{II}F_6$ entities. This can be understood by the action of the strong linear Jahn–Teller coupling in the latter cases, which produces much shorter bond lengths in the equatorial and axial directions for $d_{x^2-y^2}$ and d_{z^2} ground states, respectively, thus increasing the d covalency along the mentioned bonds. The spin transfer in $Cu(OH_2)_6{}^{2+}$ polyhedra (measured on ^{17}O) is 22%[26] as for Cu^{2+}-doped K_2ZnF_4, in accord with the nearly comparable ionicity of H_2O and F^- as ligands. For $Cu(NH_3)_6{}^{2+}$ complexes, a total spin transfer of 27% and an α value of 0.90 are reported,[27] which magnitudes nicely reflect the more pronounced covalency of the NH_3 compared to the F^- ligand of the CuF_6 centers in K_2ZnF_4 (and Ba_2ZnF_6). For the case of the equally tetragonally elongated $Cu(NO_2)_6{}^{4-}$ octahedra in various nitro complexes, a considerably enhanced total spin transfer of 39% and an α value of 0.87 is observed.[28] Indeed the N ligator atom of the NO_2^- ligand exhibits a much larger nephelauxetic effect than NH_3 (octahedral Ni^{2+}; for NH_3, β = 0.85; for NO_2^-, $\beta \approx 0.7_0$),[29] which indicates a large increase of the d covalency of the Cu–N bonds. It should further be noted, that the bond contributions from d(metal)–s(ligand) overlap are rather small for the F^- ligand. The ratio between the ligand p and s mixing coefficients in the ground-state MO of $Cu(NO_2)_6{}^{4-}$ is 1.6 and corresponds approximately to sp^2-hybridized orbitals at the nitrogen ligator atoms, while this ratio is ≳3 for F^-.

Square-planar $CuF_4{}^{2-}$ entities are only known to exist in the compounds $Ca(Sr)CuF_4$ (bond lengths 1.88 Å).[30] The molecular *g* values ($g_{\|}$ = 2.47, $g_{\perp}$ = 2.07_5)[31] are very similar to those of center II in Ba_2ZnF_6 and additionally confirm the proposed nature of the center. It should finally be mentioned that center II is not observed in the EPR spectra of powder samples $Ba_2Zn_{1-x}Cu_xF_6$, which were prepared under different experimental conditions.[1]

The results of the optical single-crystal spectroscopy will be published separately;[17] a preliminary account of the luminescence properties has been given already.[32]

Acknowledgment. We are grateful to the Humboldt Foundation and the Australian Research Grants Scheme for financial support for M.A.H. and H.S., respectively, and to the "Deutsche Forschungsgemeinschaft" and the "Fonds der chemischen Industrie".

Registry No. Ba_2ZnF_6, 18581-60-7; Cu^{2+}, 15158-11-9.

---

(26) Getz, D.; Silver, B. L. *Inorg. Chem.* **1976**, *15*, 1240.

(27) Shyr, Chin-I. Doctoral Thesis, Illinois Technical Institute, Chicago, IL, 1969.

(28) Ozarowski, A.; Reinen, D. *Inorg. Chem.* **1985**, *24*, 3860.

(29) Reinen, D.; Friebel, C.; Reetz, K. P. *J. Solid State Chem.* **1972**, *4*, 103.

(30) von Schnering, H. G.; Kolloch, B.; Kolodziejczyk, A. *Angew. Chem.* **1971**, *83*, 440.

(31) Reinen, D.; Dance, J.-M. *Inorg. Solid Fluorides* **1985**, *18*, 525.

(32) Matthies, H.; Recker, K.; Wallrafen, F.; Dirksen, G. J.; Blasse, G. *Chem. Phys. Lett.* **1988**, *149*, 167.